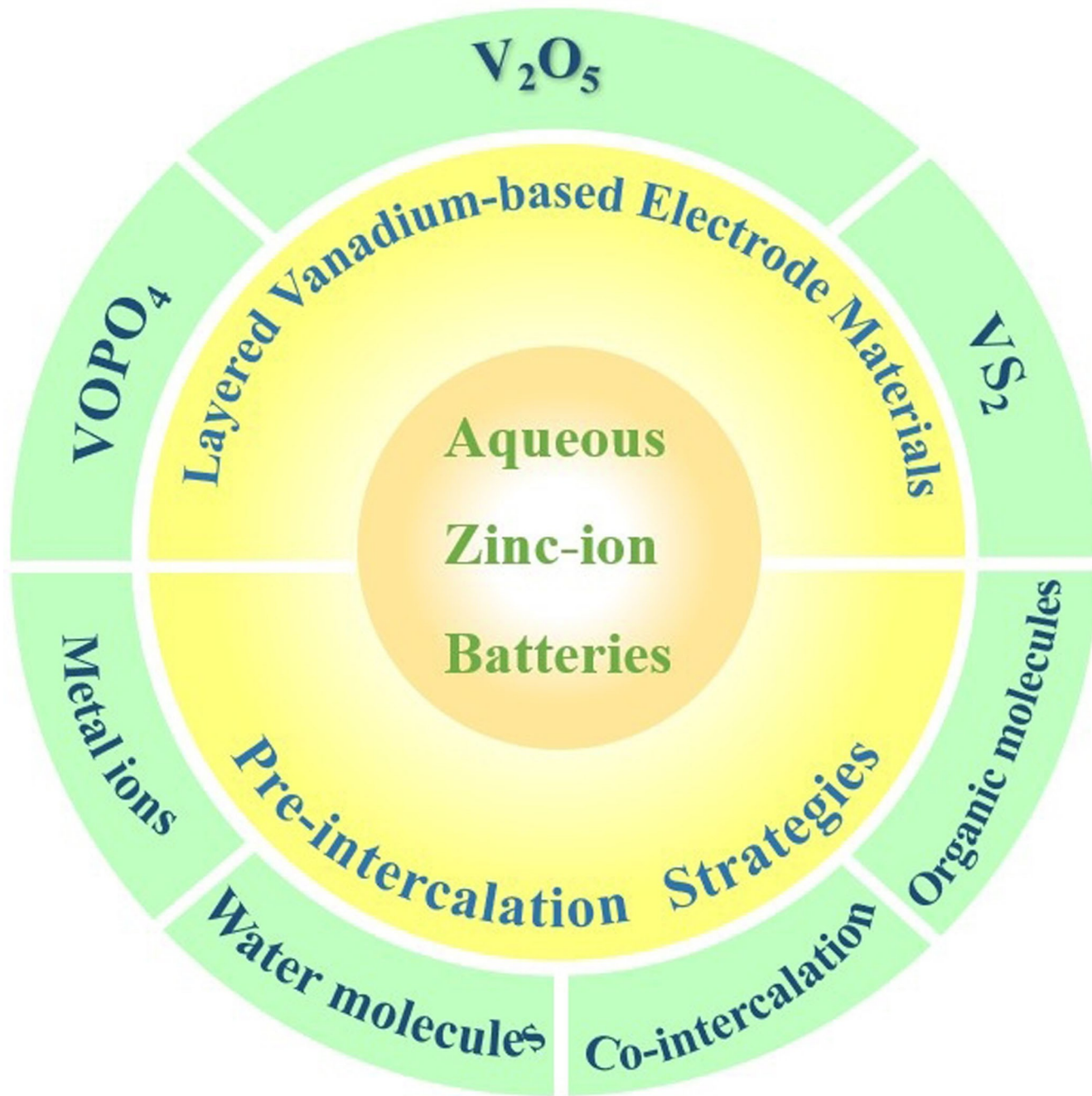


Special
Collection

Pre-intercalation Strategies to Layered Vanadium-based Electrode Materials for Aqueous Zinc Batteries

Yi Liu,^[a] Ying Liu,^[a] and Xiang Wu^{*[a]}

Aqueous zinc-ion batteries (AZIBs) have become the most potential alternatives to lithium-ion batteries (LIBs) due to their intrinsic safety, convenient operation, and environmentally friendly characteristics. Layered vanadium-based compounds with two-dimensional ion diffusion channels attract extensive attentions as cathodes for AZIBs. However, they usually suffer from dissolution and large volume change during charging/discharging. Recently, the pre-insertion strategy of guest ions or

molecules into the host has provided an effective solution. In this review, we first introduce the application and research trends of vanadium-based cathode materials for AZIBs. Then, the interlayer engineering of the pre-intercalation strategy is emphatically summarized. Finally, we propose future challenges for developing high-performance layered vanadium-based electrode materials.

1. Introduction

With the increasingly serious energy crisis, the development of energy storage technology has attracted extensive attention.^[1] LIBs dominate practical applications due to their satisfactory energy density.^[2,3] Nevertheless, the potential safety issues arising from organic electrolytes and the shortage of lithium resources limit the further utilization of LIBs.^[4] In order to seek the alternatives to LIBs, various aqueous metal-ion batteries (Na, K, Zn, Mg, Ca, Al) have been designed.^[5–10] Compared with monovalent ions, multivalent ion batteries possess high energy density because many electrons can be transferred during the electrochemical process.^[11,12] Among them, AZIBs are much significant because of their high Zn anode gravimetric capacity (820 mAh/g), ionic radius (0.74 Å) closest to Li-ion (0.76 Å), and low potential (−0.763 V vs. SHE).^[13] However, due to their high polarization characteristics and strong electrostatic interaction of Zn²⁺, it is still a challenge to develop appropriate host materials.^[14–16]

In recent years, vanadium-based compounds with diverse crystal structures have attracted conspicuous investigation (Figure 1a). It mainly includes tunnel-type structure with one-dimensional (1D) diffusion channels,^[17,18] layered structure with 2D diffusion channels,^[19,20] and NASICON-type structure with 3D diffusion channels.^[21,22] Figure 1(b) shows the overview of electrochemical performance of the above three structures. The tunnel-type and NASICON-type crystal structures possess excellent capacity retention due to large lattice tunneling and open 3D frameworks, respectively. Layered vanadium-based cathode owns large diffusion space and adjustable interlayer spacing.^[23] It can deliver considerable capacity, long cycling life and high energy density. However, the collapse of layered structure leads to their performance degradation.^[24] To tackle the problem, the modification of the adjustable and controllable interlayer (pre-intercalation) seems promising.^[25,26] It can strengthen the inherent cyclic stability on atomic scale.^[27]

In this review, we first discuss the crystal structures, electrochemical performances and reaction mechanisms of various layered vanadium-based compounds. In the following

Section, the intrinsic mechanism of layered vanadium-based compounds pre-intercalation are emphatically summarized. Finally, we present prospects for the challenges and research priorities of intercalation strategies in the future.

2. Layered Vanadium-based Cathode Materials

Layered vanadium-based compounds represented by V₂O₅, VOPO₄ and VS₂ are suitable cathode materials for AZIBs.

2.1. Layered V₂O₅ compounds

V₂O₅ with the orthorhombic phase of Pmmn (59) space group is the most common vanadium oxide.^[28] The (001) layers along the c-axis (4.4 Å) are widely spaced, which is favorable for the storage of Zn²⁺.^[29,30] Unsatisfactorily, it remains major obstacle due to the large polarization and volume changes induced by the incorporation of Zn²⁺ as a multivalent carrier into V₂O₅.^[31] Porous micro/nano-spheres can relieve the volume change and reduce the ion transport length during Zn²⁺ embedding/de-embedding.^[32] Thus far, the researchers have reported many V₂O₅ porous hollow sphere cathode materials.^[33–35] Zheng's group fabricated novel V₂O₅ yolk-shell microspheres (V₂O₅–YS) as low-cost electrode materials for AZIBs (Figure 2a).^[36] The yolk-shell structure can alleviate the structural stress raised by ion insertion/extraction during the cycling processes. From the CV curves (Figure 2b), the V₂O₅–YS cathodes undergo an activation process, and the reaction after activation is much reversible. Figure 2(c) shows a possible storage mechanism. During the first few cycles of activation, V₂O₅·nH₂O is formed with the insertion of H₂O and H⁺. Meanwhile, the Zn₃V₂O₅(OH)₂·2H₂O by-product appears due to the dissociation of water. Subsequently, the reversible insertion of Zn²⁺ occurs in V₂O₅·nH₂O.

Although the structure collapse can be significantly alleviated by constructing porous microspheres, the cyclic stability of V₂O₅-based cathodes is poor due to low charge transfer efficiency and self-aggregation during charging and discharging. Developing high conductive substrates for metal oxides is an effective method to reduce the internal resistance, thereby improving the conductivity.^[37] He et al. think that it is suitable to combine non-aggregated vertically orientated graphene (VG) with high-activity battery materials for high-durability cathodes of ZIBs.^[38] Figure 2(d) shows the schematic

[a] Y. Liu, Y. Liu, Prof. X. Wu
School of Materials Science and Engineering
Shenyang University of Technology
Shenyang 110879 (P. R. China)
E-mail: wuxiang05@sut.edu.cn

Special Collection
An invited contribution to a Special Collection on IV Symposium on Advanced Energy Storage

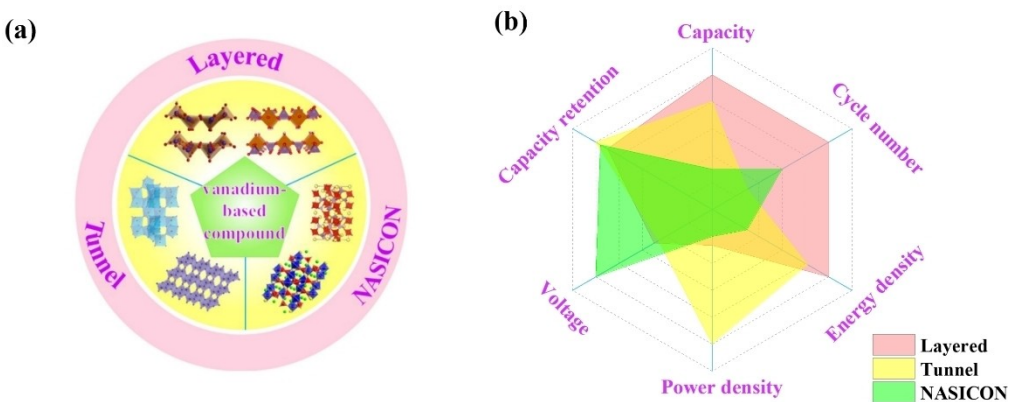


Figure 1. a) The crystal structure of vanadium-based compounds. b) The electrochemical performance of tunnel-type, layered and NASICON-type structure.

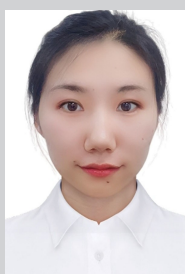
of the formation of $V_2O_5/VG/CC$ hybrid structure. A large number of graphene nanosheets are grown vertically on the carbon cloth (CC) by microwave plasma chemical vapor deposition. Subsequently, V_2O_5 nanosheets are uniformly covered on the VG surface to form a rich edge $V_2O_5/VG/CC$ hybrid cathode. The electrochemical impedance spectra in Figure 2(e) indicate that the electrode shows low charge transfer resistance. The satisfactory rate performance and cycling stability can be ascribed to their high conductivity. Also, the large surface area of VG substrate provides fast electron transfer channels.

It is also feasible to coat V_2O_5 with amorphous carbon to enhance zinc storage and electrical conductivity. Chen et al. prepared $C@V_2O_5$ cathode materials with network structure using chitosan as a template.^[39] Single-crystal V_2O_5 decorated with amorphous carbon shows an excellent electrochemical

performance. The $Zn/C@V_2O_5$ device delivers a specific capacity of 361 mAh g^{-1} at 0.5 A g^{-1} . The enhanced zinc ion storage performance features the thin amorphous carbon layer. It can significantly improve the electrical conductivity and reduce energy consumption.

2.2. Layered polyanionic compounds

Compared with V_2O_5 , $VOPO_4$ is a typical polyanion cathode. VO_6 octahedras share with each other and connect with PO_4 tetrahedras simultaneously to form layered structure and corresponding 2D diffusion channels. Chen et al. developed highly reversible AZIBs based on layered $VOPO_4$ electrode materials.^[40] Due to the presence of water in salt electrolyte, the voltage window of $Zn/VOPO_4$ batteries can be enlarged to



Yi Liu received her B.S. degree in Materials Science and Engineering from Liaoning University of Technology, China in 2020. Then she joined Prof. Xiang Wu's group in Shenyang University of Technology, China for pursuing her doctor degree in Materials Science and Engineering. Her research interest focuses on aqueous Zn ion batteries. Her research work has been reported in Journal of Colloid and Interface Science and Batteries & Supercaps and so on. She is a winner of National Scholarship for Graduates in 2021.



Ying Liu received her B.S. degree in Materials Science and Engineering from Liaoning University of Technology, China in 2018. Then she joined Prof. Xiang Wu's group in Shenyang University of Technology, China for pursuing her doctor degree in Materials Science and Engineering. Her research interest focuses on aqueous Zn ion battery and hybrid capacitor. She has published more than 10 papers such as Nano Energy, Journal of Energy Chemistry, ACS Applied Materials & Interfaces, Chinese Chemical Letters and Materials Today Energy and so on. She wins National Scholarships for Graduates in 2021 and 2022, respectively.



Dr. Xiang Wu received his Ph. D degree in Materials Science and Engineering from Harbin Institute of Technology in 2008. After that he joined Harbin Normal University until Sept. 2016. He ever worked as a visiting scientist in National Institute for Materials Science (NIMS), Japan and Taiwan University, China. He is now a full professor of materials science in Shenyang University of Technology, China. His research interests focus on synthesis, characterization of semiconductor nanomaterials and their applications in environment and energy fields. He has authored and co-authored over 170 peer reviewed journal articles. Cited time of the publications is over 7400 and H-factor is 50.

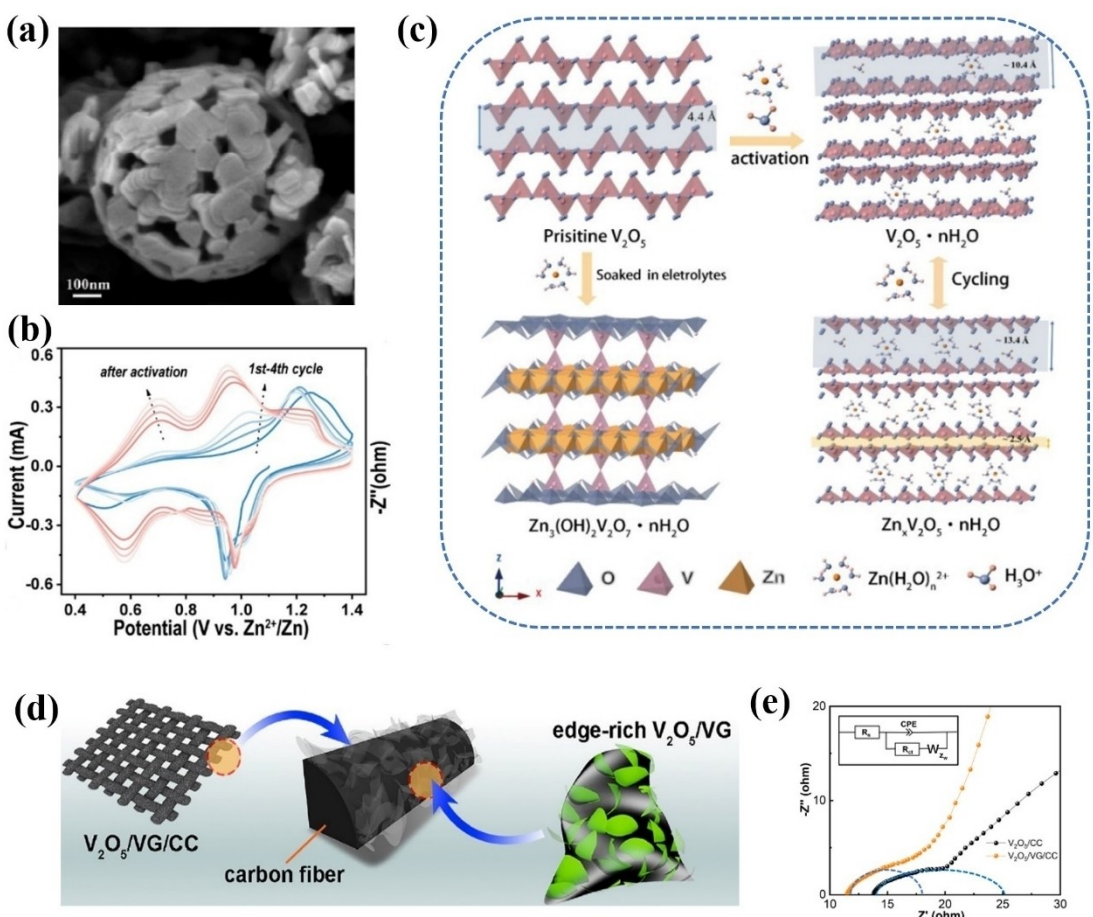


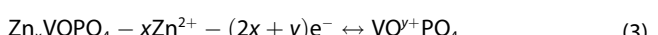
Figure 2. a) SEM image of V₂O₅ yolk-shell microsphere. b) CV curves at a scan rate of 0.1 mV s⁻¹. c) Schematic illustration of energy storage mechanism during activation and cycling process. Reproduced with permission from Ref. [36]. Copyright (2020) Royal Society of Chemistry. d) Scheme of the formation of edge-rich V₂O₅/VG/CC hybrid structure for ZIB cathode. e) EIS spectra of V₂O₅/VG/CC and V₂O₅/CC electrodes. Reproduced with permission from Ref. [38]. Copyright (2021) Elsevier B.V.

2.1 V. And the average working potential is increased to 1.56 V under the action of reactive oxygen. Figure 3(a) shows the redox mechanism of oxygen and vanadium. The reaction process is as follows:

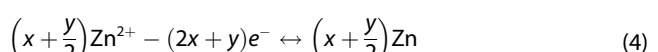
Cathode:



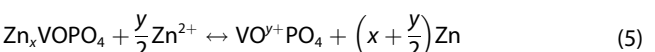
The overall reactions on cathode:



Anode:



Overall:



The oxygen redox chemistry creates extra capacity in the high-pressure region. Furthermore, it accelerates the reversible crystal structure evolution of VOPO₄ during cycling.

The layered VOPO₄ can also be modified by the interlamellar insertion of H₂O to reduce the electrostatic repulsion between the intercalated Zn²⁺ and the host. The VOPO₄·2H₂O is considered to be a promising electrode for AZIBs, Figure 3(b) shows the crystal structure of VOPO₄·2H₂O.^[41] Liang et al. utilized organic interlamellar engineering and in-situ carbonization routes to prepare the vanadyl phosphate intercalated with nitrogen doped carbon (VOP/NC).^[42] Figure 3(c) shows a rapid fabrication process of VOP/NC cathodes and pseudocapacitive Zn²⁺ memories. The modified VOP/NC possesses many reactive sites and stable structure. From Figure 3(d), the VOP/NC electrodes provide a capacity of 187.9 mAh g⁻¹ after several cycles, and sluggishly decay to 161.3 mAh g⁻¹. Furthermore, the pseudocapacitive storage mechanism promotes the intercalation kinetics of Zn²⁺. The contribution rate of capacitance

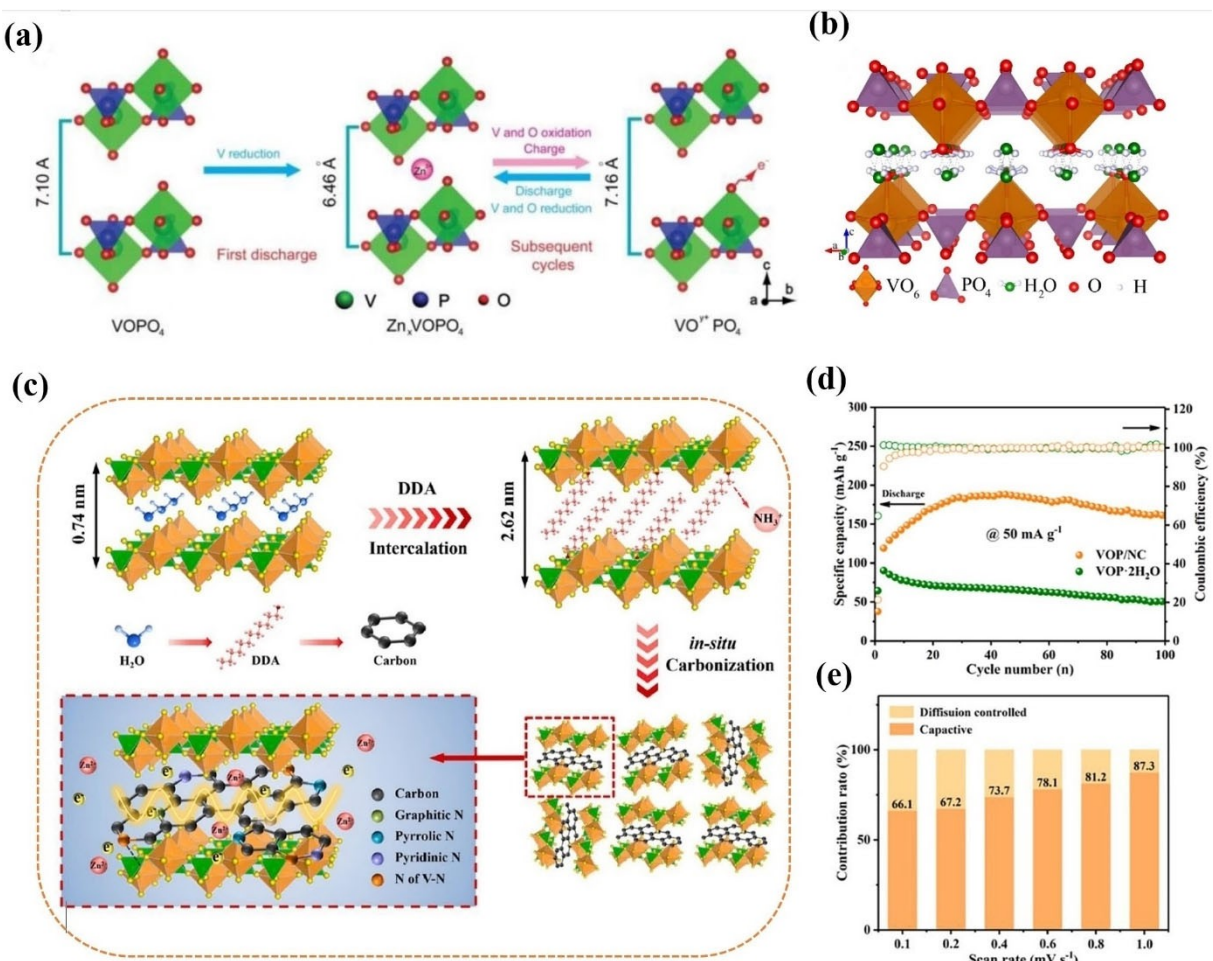


Figure 3. a) Schematic of oxygen and vanadium redox mechanism during charge/discharge process. Reproduced with permission from Ref. [40]. Copyright (2019) Wiley-VCH. b) Crystal structure of VOPO₄·2H₂O. Reproduced with permission from Ref. [41]. Copyright (2019) American Chemical Society. c) Schematic illustration of the synthesis procedure of VOP/NC cathode with fast pseudocapacitive Zn²⁺ storage. d) Cycling performance at 50 mA g⁻¹ of VOP/NC and VOP·2H₂O electrodes. e) Normalized contribution ratio of capacitive and diffusion-controlled capacities of VOP/NC at initial state. Reproduced with permission from Ref. [42]. Copyright (2021) Elsevier B.V.

reaches 87.3% at 1.0 mV/s (Figure 3e). The strategy greatly improves battery output and cycle durability.

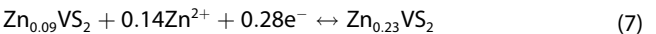
VOPO₄·2H₂O shows the disadvantage of low specific capacity as electrode materials for AZIBs. Generally, the generation of vacancies can regulate the performance of electrode materials through energy band modification. Hu et al. developed bilayer VOPO₄·2H₂O (bilayer-VOP) nanosheets with high concentration of oxygen vacancies through a simple liquid stripping strategy,^[43] as shown in Figure 4(a). From Figure 4(b), the diffusion coefficient of zinc ions in bilayer-VOP nanosheets and bulk VOPO₄ are $4.6 \times 10^{-7} \text{ cm}^{-2} \text{ s}^{-1}$ and $6.1 \times 10^{-13} \text{ cm}^{-2} \text{ s}^{-1}$, respectively. The former outperforms the latter by 6 orders of magnitude. It is proved that the reaction kinetics can be enhanced by the formation of oxygen defects. In addition, the bilayer-VOP nanosheet cathode possesses an excellent performance of 313.6 mA h g⁻¹ at 0.1 A g⁻¹. After 500 cycles, its capacity retention rate is 94.6% (296.8 mA h g⁻¹). The VOPO₄·2H₂O cathode shows serious capacity decline (only 50.7% capacity retention) under the same condition (Figure 4c).

2.3. Layered VS₂ compounds

VS₂ is a representative transition metal dichalcogenide. Its interlayer spacing is 5.7 Å, which is sufficient to realize the reversible shuttle of Zn²⁺ (0.74 Å). Mai's group constructed high-performance Zn/VS₂ batteries for the first time.^[44] The operating mechanism of the device as seen from Figure 5(a). During the cycling process, the transfer of Zn²⁺ can be divided into three steps. Firstly, there is a phase transition of VS₂ to Zn_{0.09}VS₂, and the electrochemical reaction is as follows:



This process promotes a highly reversible intercalation reaction. Next, the phase transition from Zn_{0.09}VS₂ to Zn_{0.23}VS₂ occurs:



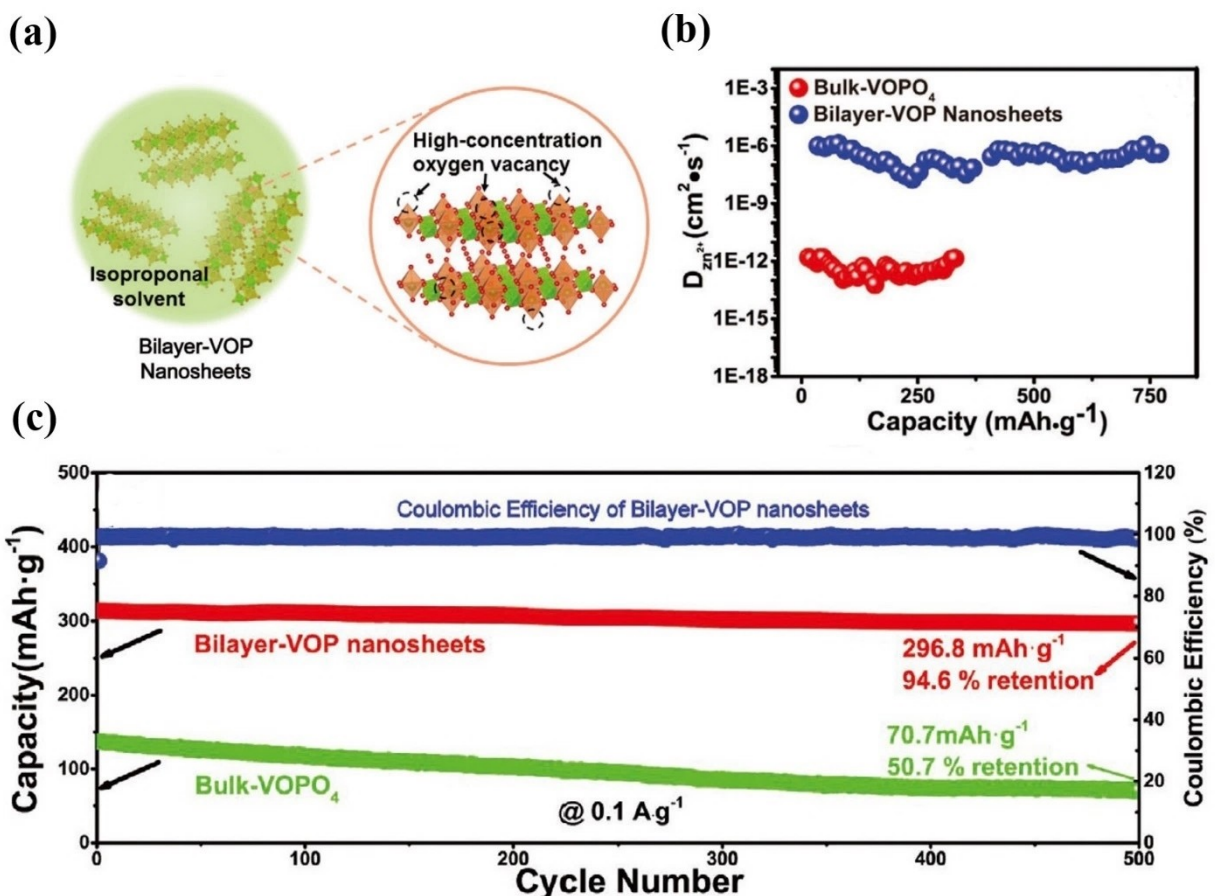


Figure 4. a) Schematic of liquid-phase exfoliation and predictable oxygen vacancy formation in bilayer-VOP nanosheets. b) Calculated zinc-ion diffusion coefficient

which provides a high capacity contribution. Finally, the VS₂ phase is gradually formed with the de-intercalation of Zn²⁺ from Zn_{0.23}VS₂ during the charging process. From Figure 5(b), the charge-discharge curves at 0.1 A g⁻¹ maintain the steady plateaus, representing the embedding and de-embedding of Zn²⁺. Nevertheless, there is a poor cycle life due to striking volume variation and low utilization of activity material.

Fan et al. alleviated the problem by using a carbon-based material (reduced graphene oxide, or rGO) as a conductive matrix.^[45] As shown in Figure 5(c), VS₂ nanosheets are overlaid uprightly on the rGO. According to HRTEM images of rGO-VS₂ composite materials (Figure 5d), the interlayer distance of VS₂ nanosheets (9.7 Å) is much larger than that of VS₂ bulk crystals (5.7 Å). The rGO-VS₂ electrode also possesses high durability as shown in Figure 5e. After several turns of activation, the capacity of electrode increases from 179 mAh/g to 190 mAh/g. A capacity retention rate of 93.3% (relative to the initial value) is obtained after 1000 cycles.

The researchers reported the direct growth of nanoflowers on stainless steel mesh grids (VS₂@SS).^[46] The design can alleviate volume expansion and thus solve the deterioration of cyclic stability with the increase of loading mass. The results show that the VS₂@SS electrodes with VS₂ loadings of 11 mg/cm² keep a 90% capacity retention (600 cycles). Importantly,

flexible solid-state batteries are assembled using VS₂@SS as the cathode in PAM (polyacrylamide)-based hydrogel electrolyte (Figure 5f). In Figure 5g, the mechanical stability of the flexible device is evaluated at different deformation angles. The GCD curves of battery change slightly at 30°, 60°, 90°, and 120°, demonstrating its application prospect in wearable electronic devices. Figure 5h demonstrates the stability of the battery at 0.5 A/g. It still possesses 91% of the initial capacity after 200 cycles.

3. Interlayer doping in layered vanadium-based materials

For layered vanadium-based compounds, the pre-intercalation of guest ions or molecules into the layered structure of the cathode can cause rearrangement of structural units and changes in interlayer space. Herein, the pre-intercalation is further divided into four parts, including metal ion, water molecule, metal ion and water molecule co-intercalation, and organic molecule pre-intercalation.

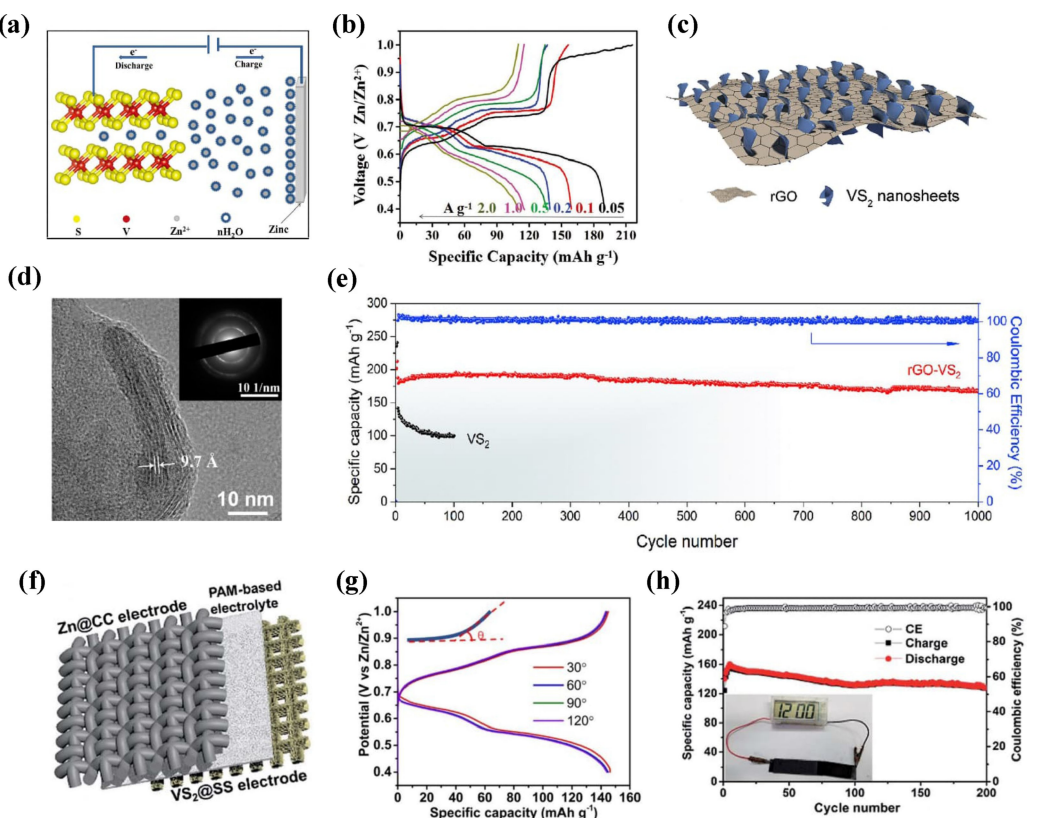


Figure 5. a) Schematic illustration of the operation mechanism of Zn/VS₂ batteries. b) Charge and discharge curves at the current density from 0.05 to 2.0 A/g. Reproduced with permission from Ref. [44]. Copyright (2017) Wiley-VCH. c) Schematic diagram of hierarchical rGO-VS₂ composites. d) HRTEM images of the rGO-VS₂ composites, inset in (d) is the corresponding SAED pattern. e) Cycling performance of rGO-VS₂ and VS₂ at 5.0 A/g. Reproduced with permission from Ref. [45]. Copyright (2020) Elsevier B.V. f) Schematic illustration of the solid-state ZIBs. g) The GCD curves of the flexible solid-state battery under various bending states at 0.5 A/g. Inset is the definition of the bending angle. h) cycling performance of the solid-state battery at 0.5 A/g (inset: an electronic watch was powered by the solid-state battery). Reproduced with permission from Ref. [46]. Copyright (2019) Royal Society of Chemistry.

3.1. Metal ions pre-intercalation

Intercalation of metal ions to form vanadate is a feasible strategy to avert collapse of layered structures. Many pre-intercalated layered vanadium-based materials have been reported successively, such as Na₃V₂(PO₄)₃,^[47] LiVOPO₄,^[48] NaVOPO₄,^[49] LiV₃O₈,^[50] Na_{1.1}V₃O_{7.9},^[51] K₂V₈O₂₁.^[52] The intercalated metal ions act as strong struts to keep the structure stable.

3.1.1. Alkali metal ions

Various alkali metal ions pre-intercalated vanadium oxides for AZIBs have been widely investigated. Kim et al. designed layered LiV₃O₈ (LVO) cathode materials.^[50] The V₃O₈ layer consists of corner-sharing VO₆ octahedra and VO₅ tetrahedrons. And the layers are linked by Li⁺ as the “pillar”. Figure 6a shows the process of Zn²⁺ insertion/extraction in LVO cathodes. The gradual phase transition occurs during Zn²⁺ insertion into LVO. At the early stage of discharge, Zn²⁺ gradually occupies Li²⁺ sites to form the ZnLiV₃O₈ phase, and phase transition towards ZnyLiV₃O₈ ($y > 1$) as discharge continues. The charging process completes the reverse transformation from ZnyLiV₃O₈ to LiV₃O₈

with the release of Zn²⁺. This zinc storage mechanism enables LiV₃O₈ to deliver a capacity of 172 mAh/g at 133 mA/g.

To study the role of interlayer metal ions in AZIBs system, Mai's group developed Na_{0.33}V₂O₅ nanowires cathode for AZIBs by the pre-intercalation of Na⁺.^[53] From Figure 6b, the Na_{0.33}V₂O₅ electrode achieves a capacity durability of 91.3% (relative to the second cycle) after 100 cycles at 0.2 A/g. The excellent performance of Na_{0.33}V₂O₅ is attributed to its high electrical conductivity. To verify the high conductivity of Na_{0.33}V₂O₅ electrode, Na_{0.33}V₂O₅ and V₂O₅ nanowire devices are also assembled and their conductivity are measured (Figure 6c and 6d). The conductivity of Na_{0.33}V₂O₅ and V₂O₅ are calculated to be 5.9×10^4 and 7.3×10^4 S/m, respectively (Figure 6e). It is proved that the intercalation of Na⁺ greatly enhances the conductivity of V₂O₅.

Compared with the above mentioned Li⁺ and Na⁺, the radius of K⁺ is large, which can efficiently decrease the electrostatic resistance of Zn²⁺ migration.^[54] Chen et al. embedded K⁺ into V₂O₅ to synthesize K_{0.5}V₂O₅ cathode.^[55] To verify the successful intercalation of K⁺, the crystal structures of V₂O₅ and K_{0.5}V₂O₅ are simulated with Vienna Ab-initio Simulation Package (VASP). In Figure 6f, V₂O₅ presents a 2D layered structure, and the atomic ratio of O and V is 5:2. In the crystal structure of K_{0.5}V₂O₅, potassium atoms are embedded between

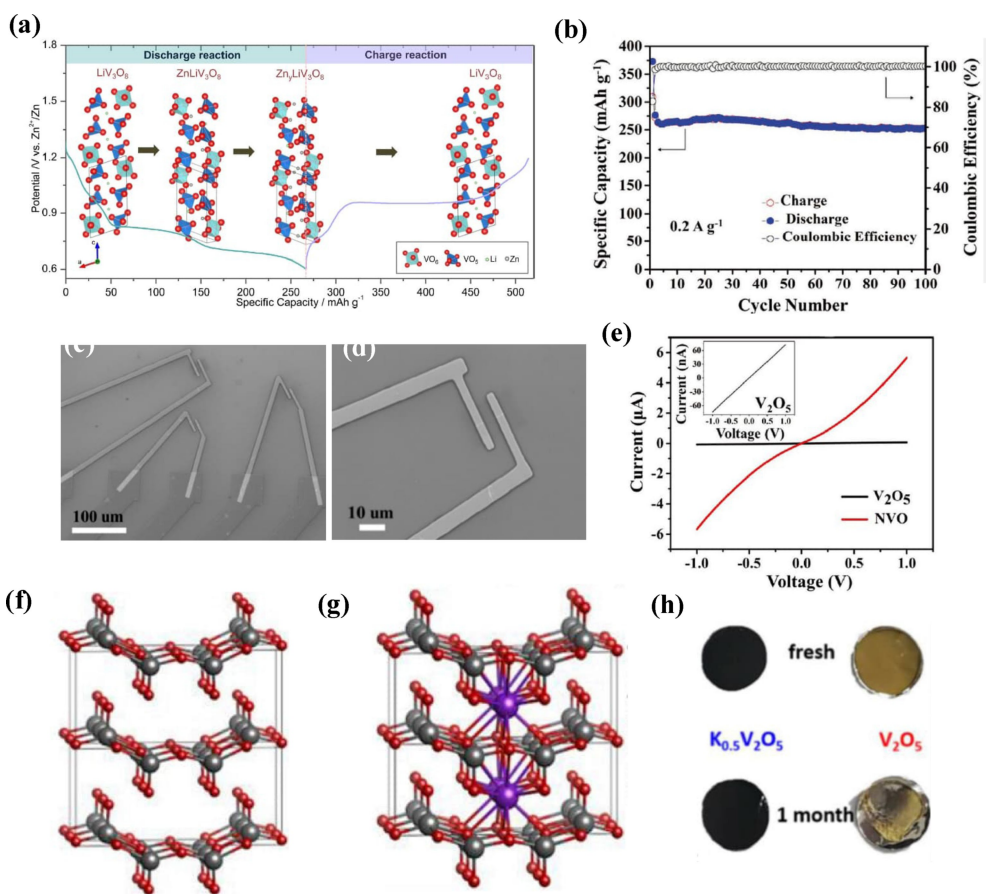


Figure 6. a) Schematic of the Zn-intercalation mechanism in the present LiV_3O_8 cathode. Reproduced with permission from Ref. [50]. Copyright (2017) American Chemical Society. b) Cycling performance of $\text{Na}_{0.33}\text{V}_2\text{O}_5$ at 0.2 A/g. c) SEM image of the NVO single nanowire device c) and d) V_2O_5 . e) The I–V curves of $\text{Na}_{0.33}\text{V}_2\text{O}_5$ and V_2O_5 . Reproduced with permission from Ref. [53]. Copyright (2018) Wiley-VCH. Illustrations of the crystal structures of f) V_2O_5 and g) $\text{K}_{0.5}\text{V}_2\text{O}_5$ predicted by using the VASP package. Red, black, and purple balls represent oxygen, vanadium, and potassium atoms, respectively. h) The appearances of $\text{K}_{0.5}\text{V}_2\text{O}_5$ and V_2O_5 cathodes after standing in 3 M ZnSO_4 for one month. Reproduced with permission from Ref. [55]. Copyright (2018) Wiley-VCH.

2D layers of V_2O_5 (Figure 6g). Single K atom combines with the oxygen atoms of the adjacent V_2O_5 layer to form a $\text{K}_{0.5}\text{V}_2\text{O}_5$ phase. The $\text{K}_{0.5}\text{V}_2\text{O}_5$ electrode remains intact after being immersed in 3 M ZnSO_4 electrolyte for 1 month. However, the V_2O_5 electrode is severely damaged by the dissolution of the electrolyte (Figure 6h). It is demonstrated that K^+ intercalation significantly improves the tolerance of $\text{K}_{0.5}\text{V}_2\text{O}_5$ in ZnSO_4 electrolyte. In addition, recent study indicates that nanoparticles can grow into nanobelts along the b axis or [010] direction with the introduction of K^+ into V_2O_5 , thereby changing the morphology and crystal structure of samples.^[56] The KVO cathode materials with exposed layer structures are expected to provide a convenient channel for Zn^{2+} (de)intercalate to realize their high-rate performance.

3.1.2. Transition metal ions

It is considered that the insertion of excessive metal ions can lead to the increase of material mass, thus reducing the specific capacity. Yang et al. studied the pre-embedding of trace transition metal ions in V_2O_5 .^[57] Figure 7a shows the XRD

patterns of samples. According to the Bragg equation, the (001) planar lattice spacings of ZnVO-300 , Fe/CuVO-300 , NiVO-300 , and Mn/CoVO-300 can be calculated 12.81 Å, 11.45 Å, 12.28 Å, and 12.41 Å, respectively. Moreover, the amount of transition metal ions and calcination temperature also affect the lattice spacing of the (001) plane (Figure 7b). In Figure 7c, long-cycle test shows that it possesses an initial specific capacity of 307 mAh/g at 10 A/g. After a small initial drop, it cycles stably for 10000 cycles with a capacity retention of 88%. From Figure 7d, the CuVO-300 cathode also achieves satisfactory rate performance at 0.5–10 A/g. As seen in Figure 7e, the EIS measurement result reveals that the charge transfer resistance of TVO-300 and VO-300 electrodes are much different, which are 350 and 1800 Ω, respectively. This is attributed to the increased electronic conductivity and interlayer spacing induced by pre-embedded guest ions.

3.2. Structural water molecules pre-intercalation

In the aqueous zinc-ion battery system, water molecules also play an important role in the structure and properties of

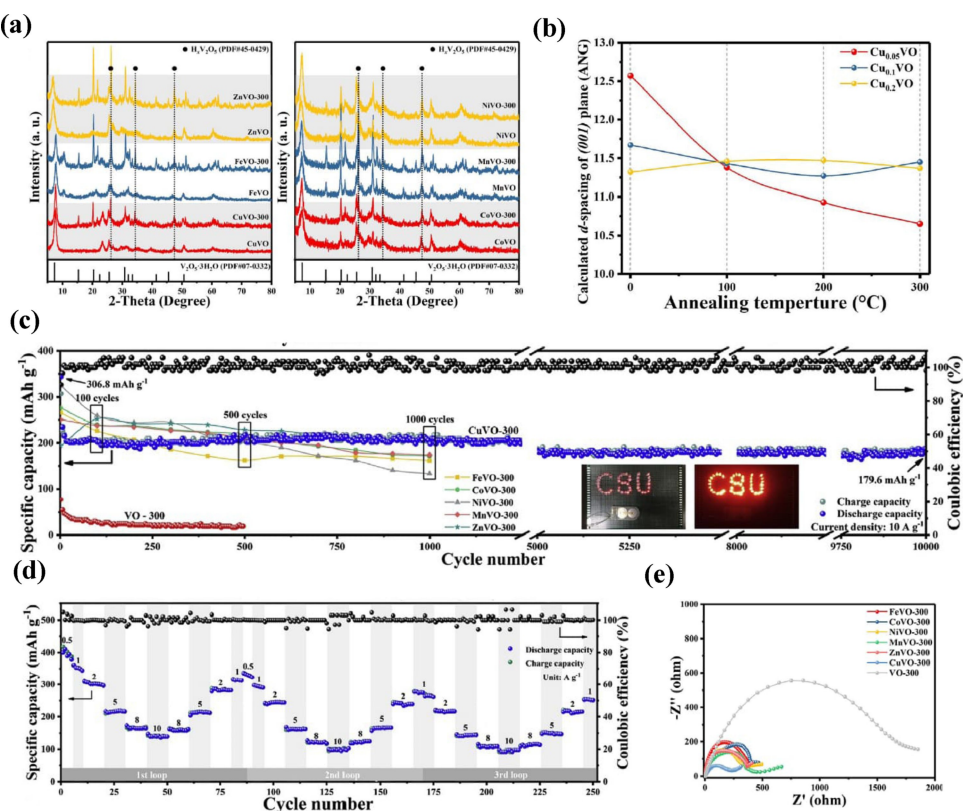


Figure 7. a) XRD patterns of TVO and TVO-300 ($T = \text{Fe}, \text{Co}, \text{Ni}, \text{Mn}, \text{Zn}, \text{Cu}$). b) corresponding calculated d spacing of (001) plane. c) Long-term cycling performances of TVO-300 and VO-300 at 10 A/g with a lamp panel illuminated by four Zn/CuVO-300 cells. d) Average discharge capacities of remaining TVO-300 at 0.5–20 A/g. e) EIS in the initial state of TVO-300 electrodes and VO-300 electrode for comparison. Reproduced with permission from Ref. [57]. Copyright (2019) Elsevier B.V.

materials. Structural water molecule can influence the electrochemical behavior of electrode materials owing to its small size and high polarity. And the charge repulsion effect can be solved by electrostatic shielding. In literature, a layered

vanadium oxide ($\text{V}_5\text{O}_{12} \cdot 6\text{H}_2\text{O}$, VOH) nanobelt was reported.^[58] It can be found from the XRD pattern that VOH possesses layered structure (Figure 8a). Water molecules increase the interlayer spacing by acting as “pillars” (11.8 Å along the direction [001])

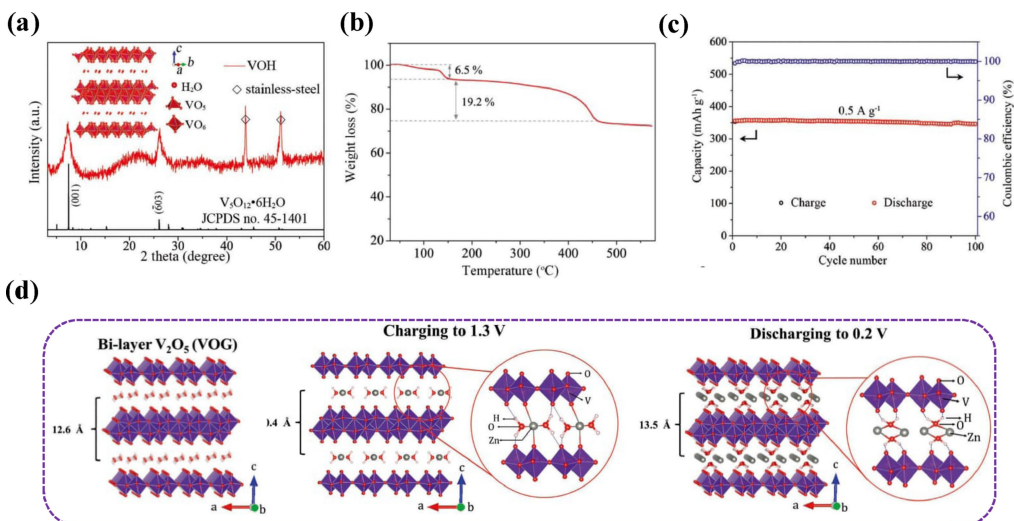


Figure 8. a) XRD pattern of VOH cathode grown on stainless-steel mesh, the inset schematically represents the layered structure of VOH. b) TG analysis of the as-prepared VOH in Ar atmosphere. c) cycling performance of the VOH cathode at 0.5 A/g. Reproduced with permission from Ref. [58]. Copyright (2019) Wiley-VCH. d) The proposed crystal structures of pristine VOG, VOG after charging to 1.3 V, and discharging to 0.2 V. Reproduced with permission from Ref. [60]. Copyright (2017) Wiley-VCH.

(axis c)). According to thermogravimetric (TG) results, the structural water of each VOH formula unit is estimated to be 5.92. In Figure 8b, the initial 6.5% weight loss is ascribed to evaporation of physically adsorbed water. Additional weight loss of 19.2% mainly corresponds to removal of crystal water. A critical problem of vanadium oxide materials is their poor capacity retention at low current density. The issue possesses its origin in structural disintegration at high degree cation intercalation (high capacities) and/or slow vanadium dissolution in mildly acidic electrolytes.^[59] The strategy of increasing layer spacing can solve the problems. From Figure 8c, the Zn/VOH battery provides a reversible capacity of 346.5 mAh/g at 0.5 A/g with a capacity durability of 97.4% after 100 cycles. Furthermore, the high coulombic efficiency (CE values ≈100%) demonstrates the improved reversibility for guest Zn²⁺ (de)intercalation.

In addition, the structural water can act as charge shielding medium in redox reaction. It can increase the interlayer distance and reduce the effective charge of Zn²⁺ through dissolution. Mai et al. studied the zinc storage capacity of bilayer V₂O₅·nH₂O.^[60] These water molecules effectively act as "lubricants" to accelerate the rapid transport of Zn²⁺ and increase the electrochemical performance. As shown in Figure 8d, the interplanar spacing is reduced from 12.6 Å nm to 10.4 Å nm after charged to 1.3 V. In the charged state, the hydrogen bonds are formed between the intercalated water molecules, electrolyte ions (CF₃SO₃⁻ and Zn²⁺) and lattice oxygen, which shortens the interlayer distance. When discharged to 0.2 V, the intercalation of hydrated zinc ions expands the interlayer spacing to 13.5 Å.

The water molecules in the electrolyte or electrodes remarkably alleviate the multivalent cation diffusion barrier. Nevertheless, their principles and mechanisms vary accordingly. On the one hand, it is believed that the lattice-structured water helps open diffusion channels, or acts as an electrostatic shield for multivalent cations.^[61,62] On the other hand, it is also thought that water molecules move with polyvalent cations.^[63] Based on the layered VOPO₄ model, Wang's group systematically studied the influence of H₂O in electrolytes and lattices on the kinetics of reversible Zn²⁺.^[64] The study shows that the H₂O at the electrolyte/electrode interface plays a significant role in the diffusion of Zn²⁺ from the electrolyte to the surface.

3.3. Metal ions and water molecules co-intercalation

Due to the high solubility of metal ions and the high polarity of water molecules, interlayer metal cation pre-intercalation is usually accompanied by co-intercalation of water molecules. The synergistic effect between metal ions and water molecules can effectively improve the performance of the cathode materials. For example, Zheng et al. synthesized Zn_{0.3}V₂O₅·1.5H₂O nanoflowers electrode materials.^[65] The co-insertion of protons and zinc ions is a common phenomenon in AZIBs. The Zn/Zn_{0.3}V₂O₅·1.5H₂O battery shows a 96% capacity retention after 20000 cycles at 10 A/g. The long cycle life can be attributed to the Zn²⁺/proton synergistic reversible inser-

tion/de-insertion mechanism. The lattice shrinkage caused by zinc intercalation and expansion induced by hydronium intercalation offsets each other and allows the lattice constant unchanged during charge and discharge. This is conducive to the cyclic stability.

The mechanism of co-intercalation of Zn²⁺ and water molecules into VOPO₄ has been reported.^[66] The layered phosphate (Zn_{0.4}VOPO₄·0.8H₂O) is synthesized by introducing Zn²⁺ into VOPO₄·2H₂O framework. The Zn_{0.4}VOPO₄·0.8H₂O electrode possesses not only a long cycle life, but also a high discharge plateau (1.45 V). The CV curves present corresponding oxidation peaks (1.5~1.7 V) and reduction peaks (1.1~1.2 V) as shown in Figure 9a. And there is an electron transfer process in a wide voltage window of 0.2~1.9 V. Furthermore, a flexible device is assembled using Zn_{0.4}VOPO₄·0.8H₂O as electrode material. From Figure 9b, two fully charged flexible ZIBs can lighten a set of LEDs in series. Even the bending angle of device changes from 0° to 45°, 90° and returns to the normal state, the LED still can emit light steadily (Figure 9c). This indicates the excellent mechanical property of the flexible battery.

Recently, theoretical calculation has become available method to confirm the Zn²⁺ storage capacity of cathode materials. He and Parkin's group designed a novel hydrated porous δ-Ni_{0.25}V₂O₅·nH₂O cathode for AZIBs.^[67] The density functional theory calculations indicate the correlation between the intercalation and diffusion properties of Zn²⁺ and the atomic arrangement of cathode. As shown in Figure 9d, when observed along the b-crystal axis, the channel I and II can be defined in the structure. Ni²⁺ occupies half of the position of channel I. And unoccupied channel II provides a pathway for Zn²⁺ migration. In addition, four possible Zn²⁺ insertion sites can be seen in Figure 9e. From Figure 9f, site A along channel I is completely filled, forming the stoichiometric relationship of Zn_{0.25}Ni_{0.25}V₂O₅·H₂O. However, Zn²⁺ can still diffuse along the channel II, proving the mechanism of further intercalation.

3.4. Organic molecules pre-intercalation

The functional groups of organic molecules can provide additional storage sites for multivalent metal ions, accompanied by electrochemically active sites increasing. Zhang et al. in situ intercalate polyaniline into layered vanadium oxide (PIVO) as cathode for AZIBs.^[68] As shown in Figure 10a, an enlarged interlayer distance (1.42 nm) is alternately constructed between the V–O layers, which provides an accelerated channel for the rapid diffusion of Zn²⁺. From Figure 10b, the XRD patterns show that the (de)intercalation of Zn²⁺ in the crystal structure of PIVO are highly reversible. More importantly, according to the change of the diffraction peaks, the increased interlayer spacing can be accumulated by many Zn²⁺, resulting in a large specific capacity. It is thought that the flexible conjugated polyaniline chains as interlayer pillars can extend the interlayer spacing of vanadium oxide. At the same time, the structural change of vanadium oxide of Zn²⁺ is buffered during the deintercalation process.

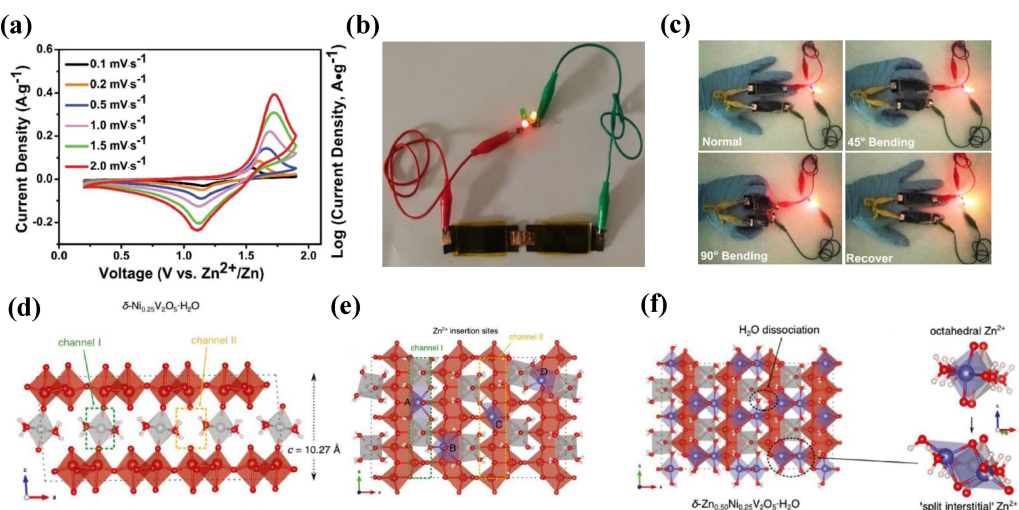


Figure 9. a) CV curves of the $\text{Zn}_0.4\text{VOPO}_4\text{-}0.8\text{H}_2\text{O}$ -based battery at different scan rates. b) Photograph of a group LEDs driven by two fully charged batteries in series. c) Exhibition of the stable output performance of the flexible batteries with different bending angles. Reproduced with permission from Ref. [66]. Copyright (2020) American Chemical Society. d) B3LYP-D3 calculated structure of $\text{Ni}_{0.25}\text{V}_2\text{O}_5\text{-H}_2\text{O}$, highlighting channels I and II. V ions are large red spheres, Ni ions are gray spheres and O ions are small red spheres, shaded regions illustrate cation coordination polyhedral. e) Intercalation sites A, B, C, and D for Zn^{2+} ions at a stoichiometry of $\text{Zn}_{0.125}\text{Ni}_{0.25}\text{V}_2\text{O}_5\text{-H}_2\text{O}$. Zn ions are blue spheres. f) Rearrangement of Zn^{2+} ions and dissociation of some H_2O in $\text{Zn}_{0.50}\text{Ni}_{0.25}\text{V}_2\text{O}_5\text{-H}_2\text{O}$. Reproduced with permission from Ref. [67]. Copyright (2020) Wiley-VCH.

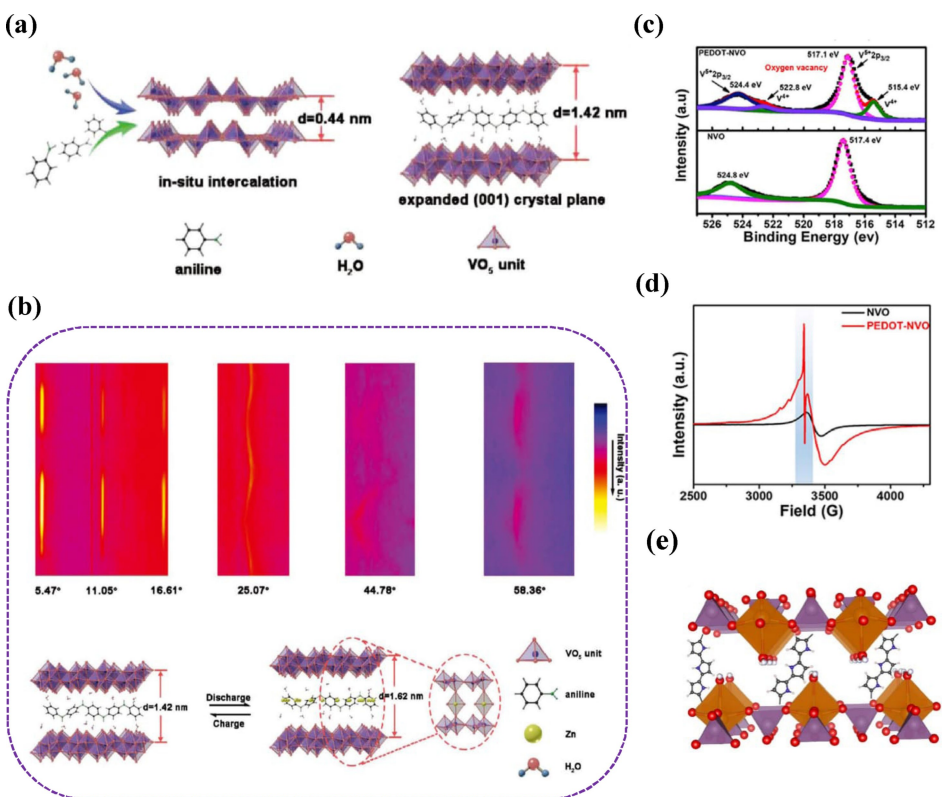


Figure 10. a) Schematic illustration for extending the interlaminar spacing of V_2O_5 via the intercalation with PANI. b) In situ XRD test and the corresponding high-resolution contour maps. Reproduced with permission from Ref. [68]. Copyright (2020) Wiley-VCH. c) High resolution XPS spectra of V 2p. d) EPR spectra with the giso-factor 2.02 highlighted by a baby-blue background. Reproduced with permission from Ref. [69]. Copyright (2020) Elsevier B.V. e) schematic for PPy-VOPO₄ showing the polypyrrole units intercalated between the VOPO₄ layers. Reproduced with permission from Ref. [41]. Copyright (2019) American Chemical Society.

The poly (3,4-ethylenedioxythiophene) (PEDOT) possesses higher stability than polyaniline. Xia et al. prepared PEDOT pre-embedded $\text{NH}_4\text{V}_3\text{O}_8$ (NVO) with an extended layer spacing of

10.8 Å (compared to 7.8 Å for single $\text{NH}_4\text{V}_3\text{O}_8$) through an effective conductive polymer intercalation.^[69] From Figure 10c, the valence state of V changes during the PEDOT intercalation

process. The mixed vanadium valence state effectively alleviates the strain during the cyclic process. Meanwhile, the electron paramagnetic resonance (EPR) result demonstrates the appearance of oxygen vacancies reduced by the polymer (Figure 10d). The PEDOT-NVO electrode can make Zn^{2+} pass through freely without destroying the structure by constructing oxygen vacancy. It shows the stable structural states and low kinetic energy barriers.

The organic molecule polypyrrole is also used as pre-intercalated species for layered VOPO₄.^[41] Figure 10e shows a schematic of polypyrrole unit embedded between the VOPO₄ layers (PPy-VOPO₄). Compared with water molecules, the binding effect between PPy molecules and VOPO₄ layers is strong, and the formed structure is much stable. Therefore, PPy-VOPO₄ possesses a smaller interplanar spacing (0.67 nm) than VOPO₄·2H₂O (0.74 nm). The pre-intercalated strategy of PPy significantly improved the electrochemical performance of VOPO₄·2H₂O. In general, a certain degree of interplanar spacing reduction will not affect the diffusion ability of Zn²⁺ in ensuring the stability of cathode host structures.

4. Conclusions and outlook

In summary, layered vanadium compounds have become promising cathode materials for AZIBs due to their 2D diffusion channels. However, their low conductivity, sluggish diffusion kinetics and poor structural stability limit further applications. Pre-intercalation of guest ions or molecules into the host and the introduction of new valence bands can improve the conductivity of layered oxide. The interlayer crystal water can shield the effective charge of multivalent metal ions, thus enhancing the diffusion kinetics. And guest metal ions or organics act as "pillars", increasing the layer spacing and significantly consolidating the crystal structure. This review introduces various layered vanadium-based cathode materials and the effect of pre-intercalation strategies on their electrochemical mechanism. Table 1 summarizes the electrochemical performance of some typical pre-intercalated vanadium-based compounds for AZIBs. Although pre-intercalation strategies have been explored for the interlayer engineering of multivalent metal ion storage, several challenges still remain (Figure 11).

Firstly, about the effect of pre-intercalation on energy storage mechanism, most researches focus on the calculation of the interlayer spacing and capacity of cathode materials. It remains controversial that whether the electrochemical performance is enhanced by the enlarging the interlayer spacing of the cathode host. Furthermore, the intercalation chemistry, diffusion kinetics, and structural stability need further investigation. The theoretical calculations also can help to understand the role of pre-intercalation.

Secondly, the hosts of pre-intercalation are mainly manganese and vanadium based layered oxides, which achieve high-capacity electrochemical performance. However, the energy density of the electrodes needs to be further improved. Increasing the working voltage is a feasible route to achieve

Table 1. The electrochemical performance of some typical guest pre-intercalated vanadium-based materials for AZIBs.

Materials	Potential window (V)	Capacity (mAh/g), Current density (A/g)	Cycle stability (current density, cycles)	Ref.
LiV ₃ O ₈	0.6-1.2	256, 0.016	75% (0.013 A/g, 65)	[50]
Li ₃ V ₂ (PO ₄) ₃	0.2-1.9	122, 60 C	74% (10 C, 4000)	[70]
Na _{0.56} V ₂ O ₅	0.4-1.5	317, 0.1	87% (1 A/g, 1000)	[71]
Na _{0.33} V ₂ O ₅	0.2-1.6	367, 0.1	93% (1 A/g, 1000)	[53]
K _{0.23} V ₂ O ₅	0.1-1.7	284, 0.1	92.8% (2A/g, 500)	[72]
K _{0.5} V ₂ O ₅	0.2-1.6	359, 1	75% (5 A/g, 3000)	[55]
V ₆ O ₁₃ ·nH ₂ O	0.2-1.4	395, 0.1	87% (5 A/g, 1000)	[73]
V ₅ O ₁₂ ·6H ₂ O	0.2-1.6	355, 0.5	94% (2 A/g, 1000)	[58]
V ₂ O ₅ ·nH ₂ O	0.2-1.6	372, 0.3	71% (6A/g, 900)	[60]
K _{1.13} V ₅ O ₁₃ ·1.3H ₂ O	0.4-1.6	444, 0.2	96.2% (10 A/g, 4000)	[74]
CuV ₂ O ₆	0.3-1.6	427, 0.1	99.3% (5A/g, 3000)	[75]
Fe _x V ₂ O ₅ ·nH ₂ O	0.3-1.4	337, 0.5	~70% (20 A/g, 1000)	[57]
Ag _{0.33} V ₂ O ₅	0.2-1.6	200, 0.2	~100% (3 A/g, 700)	[76]
δ-Ni _{0.25} V ₂ O ₅ ·nH ₂ O	0.4-1.7	402, 0.2	98% (5 A/g, 1200)	[67]
NH ₄ V ₄ O ₁₀	0.2-1.6	435, 0.2	95% (10 A/g, 1500)	[77]
Zn _{0.3} V ₂ O ₅ 1.5H ₂ O	0.3-1.6	426, 0.2	96% (10 A/g, 20000)	[65]
Zn _{0.4} VOPO ₄ ·0.8H ₂ O	0.2-1.9	162, 0.1	71.9% (0.1 A/g, 1000)	[66]
Li _{0.45} V ₂ O ₅ ·0.89H ₂ O	0.3-1.5	403, 0.1	86% (10 A/g, 1000)	[78]
Ca _{0.12} Zn _{0.12} V ₂ O ₅ ·nH ₂ O	0.3-1.7	478, 0.2	76% (10 A/g, 3000)	[79]
H ₁₁ Al ₂ V ₆ O _{23.2}	0.4-1.6	416, 0.3	≈86% (1 A/g, 3000)	[80]
PANI-V ₂ O ₅	0.4-1.6	490, 0.1	71% (1 A/g, 1000)	[81]
PEDOT-NH ₄ V ₃ O ₈	0.4-1.6	357, 0.05	94% (10 A/g, 5000)	[69]
PPy-VOPO ₄	0.5-1.8	86, 0.025	91% (0.1 A/g, 350)	[41]

the high energy density of the cells. The working voltage of AZIBs is usually lower than 2 V due to the limitation of oxygen evolution reaction. One should achieve high working voltage on the basis of high specific capacity, thereby obtaining AZIBs with high energy density.

Thirdly, the pre-intercalated guests are mainly monovalent and multivalent cations, water molecules and organic molecules. To explore the effect of guest species on the performance of zinc storage, the anions as guests should also be studied. In addition, some new pre-insertion protocols need to be developed. For example, dual ionic co-intercalation, ionic and molecular co-intercalation, and dual molecular co-intercalation. And the researchers should seek other vanadium-based layered compounds as pre-intercalation host materials. In

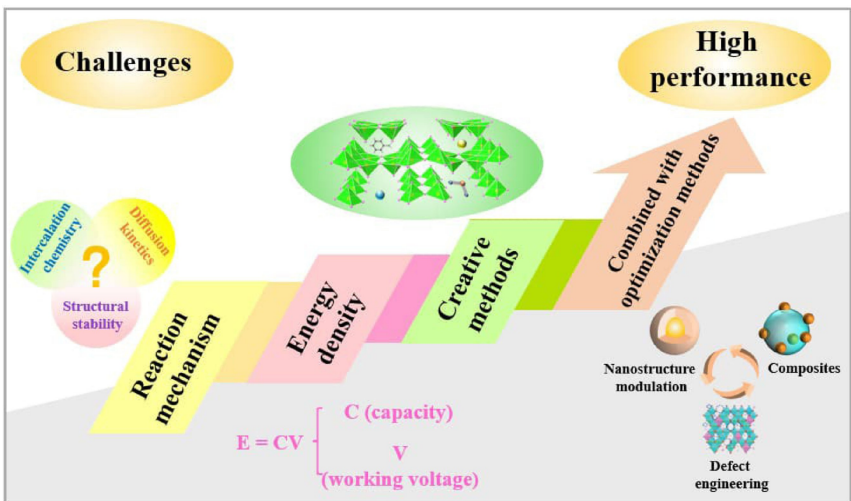


Figure 11. Future challenges for pre-insertion strategies

recent years, artificial intelligence technology has attracted extensive attention in the prediction of material properties and the development of new functional materials. It can find the correlation between properties and structures so as to design electrode materials with high performance.

Finally, to optimize the performance of cathode materials, it is not enough to only rely on the pre-intercalation strategies. It needs combine with some other optimization approaches, such as defect engineering, material composite modulation, and elemental doping etc. In battery systems, the modification of separator and interfacial energy storage can improve the overall performance of device.

Acknowledgements

The work is supported by National Natural Science Foundation of China (No. 52172218).

Conflict of Interest

The authors declare that they do not any conflicts.

Keywords: Aqueous zinc ion batteries · Layered vanadium-based compound · Pre-intercalation · Cathode materials

- [1] D. Zhao, R. Zhang, M. Dai, H. Liu, W. Jian, F. Q. Bai, X. Wu, *Small* **2022**, *18*, e2107268.
- [2] A. Masiás, J. Marcicki, W. A. Paxton, *ACS Energy Lett.* **2021**, *6*, 621–630.
- [3] X. Guo, C. Wang, W. Wang, Q. Zhou, W. Xu, P. Zhang, S. Wei, Y. Cao, K. Zhu, Z. Liu, X. Yang, Y. Wang, X. Wu, L. Song, S. Chen, X. Liu, *Nano Research Energy* **2022**, e9120026.
- [4] Y. Liu, X. Wu, *Chin. Chem. Lett.* **2022**, *33*, 1238–1246.
- [5] T. Wang, D. Su, D. Shanmukaraj, T. Rojo, M. Armand, G. Wang, *Electrochem. Energy Rev.* **2018**, *1*, 200–237.
- [6] S. Zhang, A. Teck, M. Titirici, 2021, Z. Guo, Z. Xu, M. Titirici, *Batt. Supercap.* **2021**, *4*, 663–670.
- [7] Y. Liu, P. Hu, H. Liu, X. Wu, C. Zhi, *Mater. Today Energy* **2020**, *17*, 100431.
- [8] Z. Li, X. Mu, Z. Zhao-Karger, T. Diemant, R. J. Behm, C. Kubel, M. Fichtner, *Nat. Commun.* **2018**, *9*, 5115.
- [9] S. Yamijala, H. Kwon, J. Guo, B. M. Wong, *ACS Appl. Mater. Interfaces* **2021**, *13*, 13114–13122.
- [10] J. Joseph, J. Nerkar, C. Tang, A. Du, A. P. O'Mullane, K. K. Ostrikov, *ChemSusChem* **2019**, *12*, 3753–3760.
- [11] F. Maroni, S. Dongmo, C. Gauckler, M. Marinaro, M. Wohlfahrt-Mehrens, *Batt. Supercap.* **2021**, *4*, 1221–1251.
- [12] X. Yuan, F. Ma, L. Zuo, J. Wang, N. Yu, Y. Chen, Y. Zhu, Q. Huang, R. Holze, Y. Wu, T. Ree, *Electrochem. Energy Rev.* **2021**, *4*, 1–34.
- [13] H. Ge, X. Feng, D. Liu, Y. Zhang, *Nano Research Energy* **2023**, e9120039.
- [14] Y. Liu, X. Wu, *Nano Energy* **2021**, *86*, 106124.
- [15] X. Wang, Z. Zhang, B. Xi, W. Chen, Y. Jia, J. Feng, S. Xiong, *ACS Nano* **2021**, *15*, 9244–9272.
- [16] Y. Liu, Y. Liu, X. Wu, Y. R. Cho, *ACS Appl. Mater. Interfaces* **2022**, *14*, 11654–11662.
- [17] Q. Wang, T. Sun, S. Zheng, L. Li, T. Ma, J. Liang, *Inorg. Chem. Front.* **2021**, *8*, 4497–4506.
- [18] J. Cao, D. Zhang, Y. Yue, T. Pakornchote, T. Bovornratanarak, X. Zhang, Z. Zeng, J. Qin, Y. Huang, *ACS Appl. Mater. Interfaces* **2022**, *14*, 7909–7916.
- [19] C. E. M. Lewis, J. F. S. Fernando, D. P. Siriwardena, K. L. Firestein, C. Zhang, J. E. Treifeldt, D. V. Golberg, *Adv. Mater. Technol.* **2021**, *7*, 2100505.
- [20] W. Gao, J. Michalicka, M. Pumera, *Small* **2022**, *18*, e2105572.
- [21] J. S. Ko, P. P. Paul, G. Wan, N. Seitzman, R. H. DeBlock, B. S. Dunn, M. F. Toney, J. Nelson Weker, *Chem. Mater.* **2020**, *32*, 3028–3035.
- [22] G. Li, Z. Yang, Y. Jiang, C. Jin, W. Huang, X. Ding, Y. Huang, *Nano Energy* **2016**, *25*, 211–217.
- [23] Y. Liu, X. Wu, *J. Energy Chem.* **2021**, *56*, 223–237.
- [24] Y. Zhou, F. Chen, H. Arandiyani, P. Guan, Y. Liu, Y. Wang, C. Zhao, D. Wang, D. Chu, *J. Energy Chem.* **2021**, *57*, 516–542.
- [25] Y. Tang, H. Zhang, S. Zhang, L. Li, Z. Liu, Z. Li, J. Shen, H. Shao, *Chem. Eng. J.* **2021**, *424*, 130378.
- [26] J. Feng, Z. Xiong, L. Zhao, C. Huang, H. Liu, S. Chen, Z. Wang, Q. Kuang, Y. Dong, Q. Fan, Y. Zhao, *J. Power Sources* **2018**, *396*, 230–237.
- [27] N. Bensalah, Y. De Luna, *Energy Technol.* **2021**, *9*, 2100011.
- [28] X. Xu, C. Yan, W. He, L. Xu, Z. Jiang, A. Zheng, H. Wu, M. Chen, G. Diao, *J. Power Sources* **2022**, *533*, 231358.
- [29] Y. Li, Z. Huang, P. K. Kalambate, Y. Zhong, Z. Huang, M. Xie, Y. Shen, Y. Huang, *Nano Energy* **2019**, *60*, 752–759.
- [30] D. Zhao, Q. Zhu, X. Li, M. Dun, Y. Wang, X. Huang, *Batt. Supercap.* **2022**, *5*, e202100341.
- [31] Z. Qi, T. Xiong, T. Chen, W. Shi, M. Zhang, Z. W. J. Ang, H. Fan, H. Xiao, W. S. V. Lee, J. Xue, *J. Alloys Compd.* **2021**, *870*, 159403.
- [32] Y. Liu, Y. Liu, Y. Yamauchi, Z. A. Alothman, Y. V. Kaneti, X. Wu, *Batt. Supercap.* **2021**, *4*, 1867–1873.
- [33] P. Hu, T. Zhu, J. Ma, C. Cai, G. Hu, X. Wang, Z. Liu, L. Zhou, L. Mai, *Chem. Commun.* **2019**, *55*, 8486–8489.

- [34] H. Qin, L. Chen, L. Wang, X. Chen, Z. Yang, *Electrochim. Acta* **2019**, *306*, 307–316.
- [35] F. Liu, Z. Chen, G. Fang, Z. Wang, Y. Cai, B. Tang, J. Zhou, S. Liang, *Nano-Micro Lett.* **2019**, *11*, 25.
- [36] R. Li, H. Zhang, Q. Zheng, X. Li, *J. Mater. Chem. A* **2020**, *8*, 5186–5193.
- [37] Z. Chen, V. Augustyn, J. Wen, Y. Zhang, M. Shen, B. Dunn, Y. Lu, *Adv. Mater.* **2011**, *23*, 791–795.
- [38] X. Zhang, Y. Tang, P. He, Z. Zhang, T. Chen, *Carbon* **2021**, *172*, 207–213.
- [39] C. Liu, R. Li, W. Liu, G. Shen, D. Chen, *ACS Appl. Mater. Interfaces* **2021**, *13*, 37194–37200.
- [40] F. Wan, Y. Zhang, L. Zhang, D. Liu, C. Wang, L. Song, Z. Niu, J. Chen, *Angew. Chem. Int. Ed.* **2019**, *58*, 7062–7067; *Angew. Chem.* **2019**, *131*, 7136–7141.
- [41] V. Verma, S. Kumar, W. Manalastas, J. Zhao, R. Chua, S. Meng, P. Kidkhunthod, M. Srinivasan, *ACS Appl. Energ. Mater.* **2019**, *2*, 8667–8674.
- [42] L. Ou, Z. Liu, Y. Zhou, H. Ou, J. Zhu, X. Cao, G. Fang, J. Zhou, S. Liang, *Chem. Eng. J.* **2021**, *426*, 131868.
- [43] Z. Wu, C. Lu, F. Ye, L. Zhang, L. Jiang, Q. Liu, H. Dong, Z. Sun, L. Hu, *Adv. Funct. Mater.* **2021**, *31*, 2106816.
- [44] P. He, M. Yan, G. Zhang, R. Sun, L. Chen, Q. An, L. Mai, *Adv. Energy Mater.* **2017**, *7*, 1601920.
- [45] T. Chen, X. Zhu, X. Chen, Q. Zhang, Y. Li, W. Peng, F. Zhang, X. Fan, *J. Power Sources* **2020**, *477*, 228652.
- [46] T. Jiao, Q. Yang, S. Wu, Z. Wang, D. Chen, D. Shen, B. Liu, J. Cheng, H. Li, L. Ma, C. Zhi, W. Zhang, *J. Mater. Chem. A* **2019**, *7*, 16330–16338.
- [47] K. Saravanan, C. W. Mason, A. Rudola, K. H. Wong, P. Balaya, *Adv. Energy Mater.* **2013**, *3*, 444–450.
- [48] G. He, W. H. Kan, A. Manthiram, *Chem. Mater.* **2016**, *28*, 682–688.
- [49] Y. Fang, Q. Liu, L. Xiao, Y. Rong, Y. Liu, Z. Chen, X. Ai, Y. Cao, H. Yang, J. Xie, C. Sun, X. Zhang, B. Aoun, X. Xing, X. Xiao, Y. Ren, *Chem.* **2018**, *4*, 1167–1180.
- [50] M. H. Alfaruqi, V. Mathew, J. Song, S. Kim, S. Islam, D. T. Pham, J. Jo, S. Kim, J. P. Baboo, Z. Xiu, K.-S. Lee, Y.-K. Sun, J. Kim, *Chem. Mater.* **2017**, *29*, 1684–1694.
- [51] Y. Cai, F. Liu, Z. Luo, G. Fang, J. Zhou, A. Pan, S. Liang, *Energy Storage Mater.* **2018**, *13*, 168–174.
- [52] B. Tang, G. Fang, J. Zhou, L. Wang, Y. Lei, C. Wang, T. Lin, Y. Tang, S. Liang, *Nano Energy* **2018**, *51*, 579–587.
- [53] P. He, G. Zhang, X. Liao, M. Yan, X. Xu, Q. An, J. Liu, L. Mai, *Adv. Energy Mater.* **2018**, *8*, 1702463.
- [54] Y. Liu, Y. Liu, X. Wu, Y. R. Cho, *J. Colloid Interface Sci.* **2022**, *628*, 33–40.
- [55] Y. Hao, S. Zhang, P. Tao, T. Shen, Z. Huang, J. Yan, Y. Chen, *ChemNanoMat* **2020**, *6*, 797–805.
- [56] S. Islam, M. H. Alfaruqi, D. Y. Putro, V. Soundharajan, B. Sambandam, J. Jo, S. Park, S. Lee, V. Mathew, J. Kima, *J. Mater. Chem. A* **2019**, *7*, 20335–20347.
- [57] Y. Yang, Y. Tang, S. Liang, Z. Wu, G. Fang, X. Cao, C. Wang, T. Lin, A. Pan, J. Zhou, *Nano Energy* **2019**, *61*, 617–625.
- [58] N. Zhang, M. Jia, Y. Dong, Y. Wang, J. Xu, Y. Liu, L. Jiao, F. Cheng, *Adv. Funct. Mater.* **2019**, *29*, 1807331.
- [59] L. E. Blanc, D. Kundu, L. F. Nazar, *Joule* **2020**, *4*, 771–799.
- [60] M. Yan, P. He, Y. Chen, S. Wang, Q. Wei, K. Zhao, X. Xu, Q. An, Y. Shuang, Y. Shao, K. T. Mueller, L. Mai, J. Liu, J. Yang, *Adv. Mater.* **2018**, *30*, 1703725.
- [61] Z. Rong, R. Malik, P. Canepa, G. Sai Gautam, M. Liu, A. Jain, K. Persson, G. Ceder, *Chem. Mater.* **2015**, *27*, 6016–6021.
- [62] G. Sai Gautam, P. Canepa, W. D. Richards, R. Malik, G. Ceder, *Nano Lett.* **2016**, *16*, 2426–2431.
- [63] H. J. Lee, J. Shin, J. W. Choi, *Adv. Mater.* **2018**, *30*, e1705851.
- [64] F. Wang, W. Sun, Z. Shadike, E. Hu, X. Ji, T. Gao, X. Q. Yang, K. Xu, C. Wang, *Angew. Chem. Int. Ed.* **2018**, *57*, 11978–11981; *Angew. Chem.* **2018**, *130*, 12154–12157.
- [65] L. Wang, K. W. Huang, J. Chen, J. Zheng, *Sci. Adv.* **2019**, *5*, eaax4279.
- [66] Z. Wu, Y. Wang, L. Zhang, L. Jiang, W. Tian, C. Cai, J. Price, Q. Gu, L. Hu, *ACS Appl. Energ. Mater.* **2020**, *3*, 3919–3927.
- [67] J. Li, K. McColl, X. Lu, S. Sathasivam, H. Dong, L. Kang, Z. Li, S. Zhao, A. G. Kafizas, R. Wang, D. J. L. Brett, P. R. Shearing, F. Corà, G. He, C. J. Carmalt, I. P. Parkin, *Adv. Energy Mater.* **2020**, *10*, 2000058.
- [68] S. Chen, K. Li, K. S. Hui, J. Zhang, *Adv. Funct. Mater.* **2020**, *30*, 2003890.
- [69] D. Bin, W. Huo, Y. Yuan, J. Huang, Y. Liu, Y. Zhang, F. Dong, Y. Wang, Y. Xia, *Chem.* **2020**, *6*, 968–984.
- [70] F. Wang, E. Hu, W. Sun, T. Gao, X. Ji, X. Fan, F. Han, X.-Q. Yang, K. Xu, C. Wang, *Energy Environ. Sci.* **2018**, *11*, 3168–3175.
- [71] P. Gao, Q. Ru, H. Yan, S. Cheng, Y. Liu, X. Hou, L. Wei, F. Chi-Chung Ling, *ChemElectroChem* **2020**, *7*, 283–288.
- [72] W. Zhang, C. Tang, B. Lan, L. Chen, W. Tang, C. Zuo, S. Dong, Q. An, P. Luo, *J. Alloy. Compd.* **2020**, *819*, 152971.
- [73] J. Lai, H. Zhu, X. Zhu, H. Koritala, Y. Wang, *ACS Appl. Energ. Mater.* **2019**, *2*, 1988–1996.
- [74] N. Qiu, Z. Yang, R. Xue, Y. Wang, Y. Zhu, W. Liu, *Nano Lett.* **2021**, *21*, 2738–2744.
- [75] Y. Liu, Q. Li, K. Ma, G. Yang, C. Wang, *ACS Nano* **2019**, *13*, 12081–12089.
- [76] B. Lan, Z. Peng, L. Chen, C. Tang, S. Dong, C. Chen, M. Zhou, C. Chen, Q. An, P. Luo, *J. Alloys Compd.* **2019**, *787*, 9–16.
- [77] Q. Li, X. Rui, D. Chen, Y. Feng, N. Xiao, L. Gan, Q. Zhang, Y. Yu, S. Huang, *Nano-Micro Lett.* **2020**, *12*, 67.
- [78] Y. Tong, X. Li, S. Su, J. Li, J. Fang, B. Liang, J. Hou, M. Luo, *J. Colloid Interface Sci.* **2022**, *606*, 645–653.
- [79] J. Li, N. Hong, N. Luo, H. Dong, L. Kang, Z. Peng, G. Jia, G. Chail, M. Wang, G. He, *Sci. China Mater.* **2022**, *65*, 1165–1175.
- [80] L. Xing, C. Zhang, M. Li, P. Hu, X. Zhang, Y. Dai, X. Pan, W. Sun, S. Li, J. Xue, Q. An, L. Mai, *Energy Storage Mater.* **2022**, *52*, 291–298.
- [81] W. Li, C. Han, Q. Gu, S. L. Chou, J. Z. Wang, H. K. Liu, S. X. Dou, *Adv. Energy Mater.* **2020**, *10*, 2001852.

Manuscript received: October 21, 2022

Revised manuscript received: December 1, 2022

Accepted manuscript online: December 4, 2022

Version of record online: December 15, 2022